



Examining the major contributors of ozone pollution in a rural area of the Yangtze River Delta region during harvest season

X. Pan^{1,*}, Y. Kanaya¹, H. Tanimoto², S. Inomata², Z. Wang³, S. Kudo², and I. Uno^{1,*}

¹Japan Agency for Marine-earth Science and Technology, Yokohama, Kanagawa prefecture, Japan

²National Institute for Environmental Studies, Tsukuba, Ibaraki prefecture, Japan

³State Key Laboratory of Atmospheric Boundary Layer Physics and Atmospheric Chemistry, Institute of Atmospheric Physics, Chinese Academy of Sciences, Beijing, China

* now at: Research Institute for Applied Mechanics, Kyushu University, Fukuoka prefecture, Japan

Correspondence to: X. Pan (xlpanelf@riam.kyushu-u.ac.jp)

Received: 25 August 2014 – Published in Atmos. Chem. Phys. Discuss.: 9 December 2014

Revised: 17 April 2015 – Accepted: 27 April 2015 – Published: 4 June 2015

Abstract. Open biomass burning (OBB) emits significant amounts of non-methane hydrocarbons (NMHCs), and the mixing of OBB with urban plumes could exacerbate regional ozone (O₃) pollution. In the present study, an observational field campaign was performed in a rural area at the northern edge of the Yangtze River Delta region (YRDR) from 15 May to 24 June 2010, during intensive open burning of wheat residues. The net photochemical production rate of oxidant (O_x = O₃ + NO₂) at the site was evaluated based on a box model (Regional Atmospheric Chemical Mechanism, Version 2) constrained by real-time ambient measurements (e.g., O₃, volatile organic compounds (VOCs), NO_x (NO₂ + NO), *J* values). Our results showed that both in situ photochemistry and direct transport from urban areas in the YRDR were responsible for the high O_x concentration at the site. During an OBB-impact case, net photochemical production of O_x in the daytime was pronounced, with a 6 h averaged O_x production rate of 13 ± 4 ppbv h⁻¹ (maximum value of 21 ppbv h⁻¹ at 12:00 CST). Photochemical O_x production changed from VOC-limited in the morning to NO_x-limited in the afternoon due to the rapid photochemical consumption of NO_x during the day. A combined analysis with positive matrix factorization demonstrated that O₃ pollution in the rural area of the YRDR was largely affected by urban emission, and OBB-related emissions also contributed to in situ photochemical production, particularly in the afternoon. Our study suggested that a joint effort in reducing both NMHCs (e.g., aromatics) and NO_x emissions in the urban area, as well as local OBB activities, may be effective in eliminating high-O₃ pollution risk in the rural areas of the YRDR.

1 Introduction

Ozone (O₃) is a crucial component in the troposphere and plays a key role in the atmosphere's oxidation capacity, which strongly influences the lifetime of biogenic/anthropogenic compounds and their corresponding climate forcing effects (Sitch et al., 2007). High concentrations of tropospheric O₃ are known to have serious detrimental environmental and health effects (e.g., crop yield reduction, human respiratory disorders) (Cape, 2008). In principle, the net production of O₃ is due to the presence of peroxy radicals from the photochemical oxidation of non-methane hydrocarbons (NMHCs), which disturbs the O₃–NO–NO₂ cycle, especially in urban areas where atmospheric loadings of NMHCs and the sum of NO₂ + NO (NO_x) are pronounced.

In China, the Yangtze River Delta region (YRDR) is one of the most important economic centers and is responsible for 11–12 % of total emission of NMHCs and NO_x in China (Zhang et al., 2009). These O₃ precursor emissions have increased by 71 % (NMHCs) and 89 % (NO_x) since 2000 (Kurokawa et al., 2013) due to rapid economic development in the region. Long-term observations have indicated that ground-level O₃ pollution in the YRDR has been increasing at a rate of +0.52 ppbv year⁻¹ (Wang et al., 2009) and at a rate of 2.7 % year⁻¹ in terms of variability in the daily maximum from 1991 to 2006 (Xu et al., 2008). Extreme O₃ pollution (hourly averages reaching 286 ppbv) has been reported at a suburban site near the Beijing megacity due to an abundance of local O₃ precursors (Wang et al., 2006).

Although open biomass burning (OBB) occurs sporadically and intensively, its impact on ambient O₃ levels has

been shown to be statistically evident. Onboard satellite observations have indicated that troposphere column O_3 concentrations are enhanced by 10–25 % in the downstream regions of fire (Ziemke et al., 2009). Such phenomena are supported by flight measurements (Takegawa et al., 2003), in which a clear positive correlation between O_3 and carbon monoxide (CO) measured in the OBB plume has been observed, implying that O_3 was photochemically produced from its precursors emitted from OBB. A recent study showed that methyl vinyl ketone (MVK) and methylacrolein (MACR) (photo-oxidation products of isoprene), as well as isoprene, are present at significant levels in some OBB plumes, indicating that isoprene plays an essential role in O_3 formation processes (Hornbrook et al., 2011). In China, large amounts of crop residue are burned directly in the field during harvest seasons, and such activities have remained intensive in the YRDR despite being legally banned by the government (Pan et al., 2011, 2013). Mixing of the OBB plume with anthropogenic pollutants (rich in NMHCs and NO_x) emitted from urban areas may significantly boost O_3 formation.

Recent analysis on the impact of OBB on regional O_3 production has generally been based on model simulations by manipulating the emissions of O_3 precursors from OBB, and the results have been heavily dependent on the appropriateness and accuracy of OBB information (e.g., emission strength, geographical location, duration) (Yamaji et al., 2010). However, quantitative analysis of the contribution of OBB to in situ O_3 production using field observations remains limited. In response to this limitation, a field measurement campaign was performed in a rural area of the YRDR from the middle of May to the end of June 2010. The O_3 production rate and sensitivity were investigated using the Regional Atmospheric Chemistry Mechanism (RACM version 2), which was constrained by real-time measurements of O_3 precursors, meteorological conditions, and J values. Positive matrix factorization (PMF) was adopted in this study to identify the possible sources of NMHCs at the site. Besides diagnosis of the O_3 production mechanism, this study provided recommendations to policy-makers to decrease the risk of high- O_3 pollution in rural areas of the YRDR.

2 Measurements

Field measurements of O_3 precursors were performed in a Science and Technology Zone (STZ) in a rural area of the northern YRDR (32.25° N, 121.37° E; Rudong Town, Jiangsu Province, China) in June 2010. Anthropogenic emissions in the STZ were very limited. To the west of the site, there were acres of agriculture fields with few inhabitants, and to the south of the site, there were numerous small county towns (e.g., Qidong, latitude: 31.808° N, longitude: 121.658° E) and larger cities (population > 2 million, e.g., Natong, latitude: 31.977° N, longitude: 120.900° E; Shang-

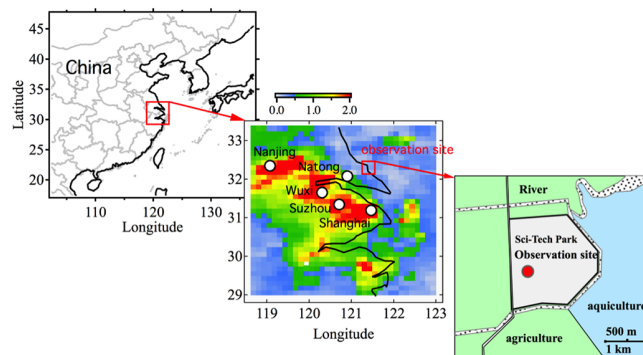


Figure 1. Geographic location of the observation site and the spatial distribution of monthly mean NO_x column density (unit: $\times 10^6$ molecule cm^{-2} , the data were derived from OMI observations, DOMINO version 2.0, <http://www.temis.nl/airpollution/no2.html>) during the field campaign period and the surrounding environment at the site.

hai, latitude: 31.246° N, longitude: 121.467° E). Emissions from industrial/residential areas of these cities could be responsible for the observed NO_x and NMHCs at the site. The geographic information for the observation site is shown in Fig. 1. In this study, the mixing ratio of O_3 was measured using a commercial UV-absorption O_3 analyzer (model 49c, time resolution: 1 min; zero noise: 0.25 ppbv with 1 min average; Thermo Scientific Inc.). The ambient CO mixing ratio was measured using a gas filter non-dispersive infrared CO gas analyzer (model 48c, zero noise: 0.04 ppm with 30 s average; Thermo Scientific Inc.). The zero point was periodically checked during the initial 20 min of each hour using purified air produced by a heated Pt catalyst (model 96; Thermo Electron Co.). Span calibrations were performed on site with standard span gas (2.03 ppmv, produced by Nissan-Tanaka Corp., Japan). Mixing ratios of NO and NO_2 were detected using a commercial NO_x analyzer (model 42CTL; Thermo Scientific Inc.). We used two converters in parallel that were switched from one to the other, a molybdenum converter for measurements of NO_y (sum of NO_x , HNO_3 , N_2O_5 , PAN, etc.) and a photolytic converter for selective measurements of NO_2 . The precision of the instrument is 0.4 ppbv with a zero noise of 0.2 ppbv with a 1 min average. The instruments were placed in a temperature-controlled container and ambient air was drawn into the room through a 2.5 m-long, 1/4 inch Teflon tube.

A total of 15 NMHC species (see Table 1) were detected using online gas chromatography–flame ionization detection (GC-FID) and gas chromatography–mass spectrometry (GC-MS) at a time resolution of 1–2 h. During measurement, ambient air was first directed to a pre-concentration unit (GAS-30; DKK-TOA Corp., Ltd., Japan) with a sampling time of 10 min. Valves and transfer lines were maintained at 80 °C to minimize the loss of VOCs in samples, and the trapping tube was held at approximately –78 °C us-

Table 1. Statistics on the mixing ratios of NMVOC species and NO₂ (in unit of ppbv), and mass concentration of BC (in unit of μg m⁻³) during the field campaign period.

Species	Average	SD	Max.	Min.	Median	10th percentile	90th percentile
Propane	1.2	2.2	4.9	0.01	0.5	0.14	2.5
Propylene	0.7	1.5	8.2	0.01	0.2	0.08	1.4
<i>i</i> -Butane	0.9	1.1	5.5	0.00	0.4	0.12	2.2
<i>n</i> -Butane	1.3	1.6	7.6	0.02	0.7	0.11	3.6
<i>t</i> -2-Butene	0.1	0.2	1.8	0.00	0.1	0.03	0.2
1-Butene	0.2	0.4	3.1	0.01	0.1	0.02	0.4
<i>c</i> -2-Butene	0.1	0.1	0.7	0.00	0.0	0.01	0.1
<i>i</i> -Pentane	0.8	0.7	4.0	0.09	0.6	0.25	1.6
<i>n</i> -Pentane	0.4	0.3	1.9	0.04	0.3	0.11	0.7
Isoprene	0.2	0.1	0.6	0.01	0.1	0.03	0.3
Benzene	1.0	0.9	4.4	0.06	0.7	0.19	2.4
Toluene	3.5	5.1	23.8	0.01	1.8	0.17	7.7
Ethyl-benzene	1.3	2.1	15.5	0.00	0.5	0.05	4.7
<i>m-p</i> -Xylene	0.7	1.3	5.9	0.00	0.2	0.03	2.8
<i>o</i> -Xylene	0.5	0.8	3.5	0.00	0.2	0.01	2.0
Furan	1.0	0.8	4.8	0.00	0.8	0.20	1.9
Acetonitrile	0.3	0.2	1.0	0.05	0.3	0.13	0.7
Acetaldehyde	3.4	2.6	15.8	0.07	2.7	0.86	7.6
Acetone/Propanal	4.2	2.6	13.4	0.53	3.6	1.51	8.3
Acetic acid	3.0	2.3	15.5	0.45	2.1	1.03	6.6
MVK/MACR	0.8	0.5	2.3	0.07	0.7	0.27	1.6
MEK/Butanal	1.1	1.1	5.4	0.09	0.7	0.30	2.6
BC	2.2	1.9	12.5	0.03	1.4	0.50	5.5
NO ₂	7.8	11.9	58.4	0.01	2.5	0.29	27.6

ing liquid carbon dioxide. Calibration of the GC/FID/MS was performed using a gas standard of 1 ppm containing 58 VOC components (PAMS-J58; Sumitomo Seika Chemicals Corp., Ltd., Japan). The detection limit of NMHCs by GC-MS was 0.002–0.005 ppbv at a signal/noise ratio of 3 (Kudo et al., 2014). Six oxygenated volatile organics and acetonitrile (See Table 1) were also concurrently measured using a commercially available proton transfer reaction mass spectrometer (PTR-MS; Ionicon Analytik GmbH, Austria). The detection limit of PTR-MS was 0.01–0.08 ppbv, and the uncertainty of the measurements was estimated to be less than 15%. The spectral actinic flux was measured using a single monochromator/photodiode array instrument (Meteorologie Consult Inc., Germany) with a wavelength ranging from 274 to 698 nm. The uncertainty in the photolysis of O₃ (J_{O^1D}) for a similar instrument has been estimated to be 14%. Chemical composition and the size distribution of aerosol particles were also measured during the field campaign. Detailed descriptions of these methods can be found in previous reports (Pan et al., 2012).

3 Methodologies

3.1 Observation-based simulation of O₃ production

The simulation of O₃ photochemistry was based on a photochemical box model, RACM version 2, which was recently released (Goliff et al., 2013). Compared with its previous version (RACM version 1) (Stockwell et al., 1997), the new version has expanded aromatic chemistry with a greater number of species, and additional and separate reaction schemes for benzene, *m*-xylene, *p*-xylene, and *o*-xylene chemistry. This mechanism employs 363 reactions and 120 species. In the calculations, O₃, NO, NO₂, SO₂, CO, and J values, as well as NMHC species, were processed into a data set with a time resolution of 10 min. The missing data (between 13 and 17 June 2010) due to instrumental maintenance were linearly interpolated but not included in the analysis. Concentrations of all species at 00:00 CST were considered the initial condition, and the integration was conducted repeatedly with an integration step of 0.01 s five times on each day. Results of the last 24 h were used as the output of simulations after the stabilization of unmeasured species. The mixing ratio of NO was assumed to be 0.01 ppbv when the observation was below the detection limit. O₃ photochemistry during the daytime (06:00–18:00 CST) was manifested based on the constrained steady-state calculation. Since NO₂ existed at high

concentrations comparable to O_3 at the observation site, the instantaneous net O_x ($O_3 + NO_2$) production rate ($P(O_x)$) was estimated by subtracting its loss ($D(O_x)$) from the gross formation rate, $F(O_x)$. The formulae are given by the following:

$$F(O_x) = k_1 [HO_2][NO] + \sum k_{2i} [RO_2]_i [NO] \phi_i \quad (1)$$

$$D(O_x) = k_3 [O^1(D)] [H_2O] + k_4 [OH][O_3] + k_5 [HO_2][O_3] + \sum k_{6j} [O_3][olefin]_j + \sum k_7 [OH][NO_2] \quad (2)$$

$$P(O_x) = F(O_x) - D(O_x), \quad (3)$$

where RO_2 represents organic peroxy radicals (e.g., CH_3O_2), ϕ represents yield of NO_2 from the $RO_2 + NO$ reactions, $[X]$ is the number density of species X , and k_1 – k_7 are the reaction rate coefficients for the $[X][Y]$ reaction. $F(O_x)$, $D(O_x)$, and $P(O_x)$ are calculated after the production and loss rates of the peroxy radicals are in balance. Although some unmeasured NMHC species impact the $P(O_x)$ calculations based on the RACM model, they do not change our major conclusions in the present study.

3.2 PMF analysis

Positive matrix factorization (PMF, version 5.0) is an advanced receptor model that analytically decomposes an $n \times m$ dimension matrix of observations into several factors (p), the species profile (f) of each source, and the amount of mass concentration (g) by solving a constrained and weighted least-squares optimization equation, as follows:

$$x_{ij} = \sum_{k=1}^p g_{ik} f_{kj} + e_{ij}, \quad (4)$$

where i and j represent the number of samples and chemical species that were measured, respectively, and e_{ij} is the residual for each sample/species. The PMF solution minimizes the object function Q , as follows:

$$Q = \sum_{i=1}^n \sum_{j=1}^m [e_{ij}/u_{ij}]^2, \quad (5)$$

where u_{ij} is the uncertainty for each samples/species. This approach integrates non-negativity constraints into the computation to make the results physically meaningful and explainable. A detailed description of the model is available in the user's guide (<http://www.epa.gov/heasd/research/pmf.html>).

3.3 Footprint analysis

An ensemble simulation of a 72 h back trajectory of air masses was performed using the Hybrid Single Particle Lagrangian Integrated Trajectory model (HYSPLIT; <http://ready.arl.noaa.gov/HYSPLIT.php>) by offsetting the meteorological data using a single meteorological grid point in the horizontal and 0.01 sigma units (approximately 250 m) in the vertical. Input meteorological data were provided by the NCEP Global Data Assimilation System (GDAS) model with a grid resolution of $1^\circ \times 1^\circ$. To better review the impact of emissions on the surface layer, only the footprint region of the air mass was demonstrated. Here, the footprint region was determined as the grids in which the geographical height of the trajectory point was lower than the mixing height in the meteorological field. The footprint region was generally consistent with the spatial distribution of source–receptor relationships determined using the FLEXPART (<http://flexpart.eu/>) dispersive model (Pan et al., 2012).

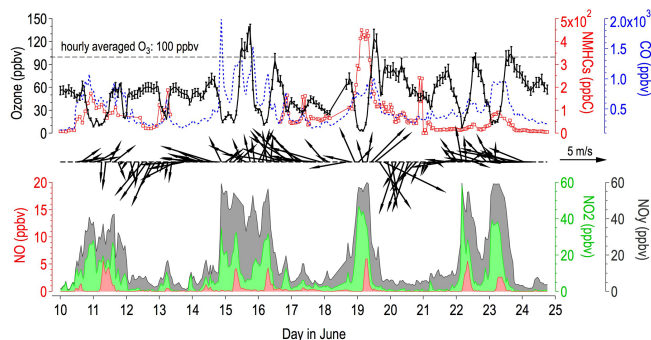


Figure 2. Time series of O_3 , CO, NMHCs, NO, NO_2 , NO_y and wind information at the site during the field campaign.

//ready.arl.noaa.gov/HYSPLIT.php) by offsetting the meteorological data using a single meteorological grid point in the horizontal and 0.01 sigma units (approximately 250 m) in the vertical. Input meteorological data were provided by the NCEP Global Data Assimilation System (GDAS) model with a grid resolution of $1^\circ \times 1^\circ$. To better review the impact of emissions on the surface layer, only the footprint region of the air mass was demonstrated. Here, the footprint region was determined as the grids in which the geographical height of the trajectory point was lower than the mixing height in the meteorological field. The footprint region was generally consistent with the spatial distribution of source–receptor relationships determined using the FLEXPART (<http://flexpart.eu/>) dispersive model (Pan et al., 2012).

4 Results

4.1 Overview of observations

Temporal variations of the mixing ratios of O_3 , NMHCs, NO_x , NO_y , CO, and wind speed and direction are shown in Fig. 2. Statistics on the NMHC species are listed in Table 1. During the observation periods, five pollution episodes (10 to 12, 14 to 17, 18 to 20, 22, and 23 June in 2010) were clearly identified based on NO_x variations, and on 4 different days (15, 19, 22 and 23 June, the hourly averaged O_3 mixing ratio exceeded 100 ppbv (dashed line as shown in Fig. 2). The highest O_3 concentration (hourly mean: 140 ± 3 ppbv) occurred at 17:00 CST on 15 June 2010. We found that the observation site was affected by the intensive open burning of crop residues in the surrounding agricultural according to the sharp increase in ambient CO levels. The hourly CO mixing ratio at 12:00 CST on 15 June was as high as 1309 ± 91 ppbv. O_3 precursors flowed out from the urban areas to the south also contributed to the build-up of ambient O_x at the site, because obvious enhancements in the NO_x mixing ratio (hourly mean: 22 ± 13 ppbv) were observed with the prevailing southerly wind (SE–SW sector), and the ambient O_3 mixing ratio decreased to almost zero due to titration

reactions when the nitrogenous species were preferentially present in the early morning pollution days. The maximum concentration of NMHCs (hourly value: 443 ppbC) occurred at 07:00 CST on 19 June when the hourly averaged NO_x and NO_y mixing ratios were 42 ± 2 ppbv and 60 ± 1 ppbv, respectively, and the hourly O_3 mixing ratio was found to be 124 ± 5 ppbv at 12:00 CST due to strongly photochemical processes in the daytime. It was worth noting that the field campaign was just within the period of Shanghai World Expo 2010. Space-based observations demonstrated that tropospheric NO_2 column loading and CO concentration at 700 hPa decreased by 8 and 12 % over the YRDR, compared with the past 3 years, probably due to short-term strict emission control measures (Hao et al., 2011). The variation in NMHC concentration during the Shanghai World Expo 2010 has not yet been reported. The effect of emission regulatory measures over the YRDR on the variability of O_3 production potentials was out of the scope of this study, although tropospheric O_3 precursors may be higher if no emission control policy is implemented.

4.2 Diurnal pattern

Figure 3 shows the average diurnal variations in O_x , CO, NO, NO_x , NO_y , $\text{NO}_z (= \text{NO}_y - \text{NO}_x)$, $\text{NO}_x / \text{NO}_y$, and NMHCs for days when the maximum hourly averaged O_x concentration was greater than 100 ppbv (red dotted lines) and those days when it was less than 100 ppbv (blue dotted lines). The hourly averaged O_x in high- O_3 pollution days showed a predominant single peak distribution with a daytime increase of 94 ppbv (Fig. 3a), reflecting of a significant depletion of O_3 at night and strong photochemical production of O_3 during the daytime due to the presence of high concentrations of O_3 precursors. In contrast, O_x levels on the low- O_3 pollution days showed a moderate increase at noontime with a daytime increase of only 24 ppbv. Variation in NO (Fig. 3b) showed a prominent peak at 07:00 CST, especially on the high- O_3 pollution days (maximum: 4.2 ± 1.2 ppbv). On the low- O_3 pollution days, the hourly averaged NO showed a weak peak (1.1 ± 1.5 ppbv). Diurnal variations in NO_2 at the site showed evident increases at night with a predominant peak (39 ± 18 ppbv) at 04:00 CST, distinct from the features (two peaks at 09:00 and 18:00 CST during rush hour) observed at the urban site of the Shanghai megacity. This implied that the NO_x was mostly transported to the observation site. A similar pattern was observed with the diurnal variation in NO_y (Fig. 3d) on high- O_3 pollution days, in that it showed a broader peak (54 ± 6 ppbv) from 04:00–09:00 CST and gradually decreased to 26 ± 3 ppbv at 15:00 CST in the afternoon. As expected, NO_z showed an obviously unimodal distribution (Fig. 3f) with a maximum value of 33 ± 10 ppbv at 12:00 CST when O_3 photochemistry was proactive. We did not observe a clear increase in either NO_y or NO_z for the low- O_3 pollution days.

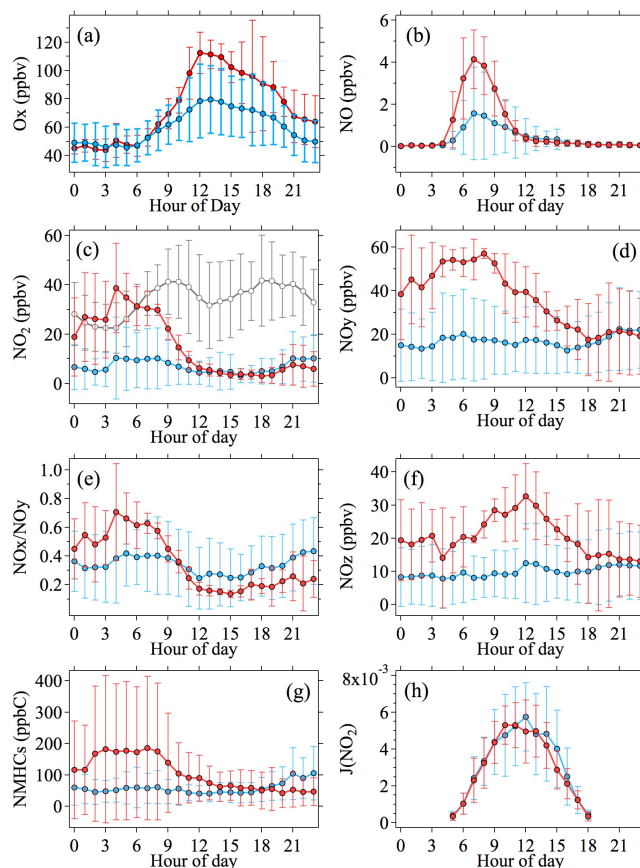


Figure 3. Diurnal variation in O_x , NO, NO_2 , NO_y , $\text{NO}_x / \text{NO}_y$, NO_z , NMHCs, and $J(\text{NO}_2)$ during the field campaign. The red and blue colors represent the averaged diurnal patterns for the high- O_3 pollution (hourly O_3 mixing ratio > 100 ppbv even only once in a day) and low- O_3 pollution (hourly O_3 mixing ratio < 100 ppbv) days, respectively. The gray line in (c) indicates the NO_2 concentration in the downtown area of the Shanghai megacity.

Diurnal variation in the $\text{NO}_x / \text{NO}_y$ ratio is illustrated in Fig. 3e. In general, a higher $\text{NO}_x / \text{NO}_y$ ratio indicates that pollution plumes have a shorter photochemical age. In the present study, we found that the plumes on high- O_3 pollution days were not photochemically aged ($\text{NO}_x / \text{NO}_y$ ratio > 0.5) when they were transported to the observation site in the morning, and they gradually became aged ($\text{NO}_x / \text{NO}_y = 0.2$) due to strong photochemical processes in the daytime. For low- O_3 pollution days, the $\text{NO}_x / \text{NO}_y$ ratio did not vary significantly and had a mean of 0.34 ± 0.1 .

As shown in Fig. 3g, the total NMHC concentration on the high- O_3 pollution days and total hourly averaged NMHC concentration varied significantly (91–447 ppbC) in the early morning (00:00–06:00 CST), and it decreased gradually to 65 ± 55 ppbC in the afternoon (12:00–18:00 CST). On low- O_3 pollution days, the NMHC concentration was constantly low with a mean of 58 ± 46 ppbC, implying that the contribution from the transport of urban emissions was less im-

portant. Diurnal variations in $J(\text{NO}_2)$ on the high- O_3 and low- O_3 pollution days during observation periods (Fig. 3h) showed nearly the same behavior, implying that the significant enhancement of O_x production during the high- O_3 pollution period did not result from variations in solar radiation.

4.3 Identification of source regions

To identify the major source regions for O_3 precursors, the color-shaded polar graph for O_3 , NO , NO_2 , NMHCs, NO_x/NO_y and NMHCs/NO_x is shown in Fig. 4. We found that a weak southerly wind ($\sim 3 \text{ m s}^{-1}$) was mostly accompanied by the occurrence of high- O_3 pollution at the site (Fig. 4a), suggesting that in situ photochemistry was important, and the high- O_3 concentration from the north and east was normally related to stronger winds ($> 5 \text{ m s}^{-1}$), implying the potential contribution from direct transport. High concentrations of NO_x (Fig. 4b, c) and NMHCs (Fig. 4d) at the site were also related to emissions from the urban/industrial areas to the south. Figure 4e shows that air masses from the west and south normally were less photochemically processed, with an NO_x/NO_y ratio larger than 0.5, especially during the high- O_3 pollution days when the NO_x/NO_y ratio was greater than 0.8.

The NMHCs/NO_x ratio partially reflected the characteristics of emission sources and corresponding O_3 production potentials. The dependence of NMHCs/NO_x on wind direction is shown in Fig. 4f. As demonstrated, the air masses from the north normally had high NMHCs/NO_x ratios with a mean of $50 \pm 44 \text{ ppbC ppb}^{-1}$. Nevertheless, typically low NMHCs/NO_x ratios ($8 \pm 7 \text{ ppbC ppb}^{-1}$ on average) were observed in the present study for plumes transported from the urban areas to the south. Ran et al. (2009) reported an average NMHCs/NO_x ratio of 8 ppbC ppb^{-1} for pollution in the downtown area of the Shanghai megacity, generally consistent with our observations. For a detailed discussion on the dependence of O_3 production on the NMHCs/NO_x ratio, see Sect. 5.3.

5 Discussion

5.1 Net photochemical production rate of O_x

The net photochemical production of O_x ($\text{P}(\text{O}_x)$) during the field campaign was calculated based on Eqs. (1)–(3). Figure 5 shows the diurnal variations in $\text{P}(\text{O}_x)$ for three high- O_3 pollution days. As shown in Fig. 5a and d, when the site experienced prevailing moderate southwest winds ($\sim 4 \text{ m s}^{-1}$) on 19 June 2010, the observed maximum O_x concentration was 128 ppbv at 12:00 CST, with a daytime increase of 79 ppbv. $\text{P}(\text{O}_x)$ also peaked (21 ppbv h^{-1}) at 12:00 CST with an accumulated photochemical production of O_x (06:00–12:00 CST) of 73 ppbv. This indicated that in situ photochemistry almost fully explained the buildup of O_x at the site in the morning. In the afternoon, the O_x concentration decreased quickly to

52 ppbv (at 17:00 CST) when it changed to a strong westerly wind ($\sim 6 \text{ m s}^{-1}$), and the total in situ photochemical production of O_x was only 27 ppbv, reflecting the importance of direct transport. Footprint calculations (Fig. 6f) indicated that O_x formation at the urban area to the south of the observation site had a significant contribution. Total O_x production was found to be 100 ppbv on a daily basis, and the 6 h (09:00–15:00 CST) averaged $\text{P}(\text{O}_x)$ was $13 \pm 4 \text{ ppbv h}^{-1}$, which was similar to the observations (13 ppbv h^{-1}) in central Tokyo areas during the summer (Kanaya et al., 2008). On 23 June (as shown in Fig. 5c and f), the daytime maximum $\text{P}(\text{O}_x)$ was found to be 19 ppbv h^{-1} at 11:00 CST. The accumulated photochemical production of O_x (06:00–11:00 CST) at the site was 41 ppbv, similar to the observed increase of O_x (48 ppbv) during this period, which indicated that the buildup of O_x could be attributed to in situ photochemistry. During the afternoon, the wind direction shifted from south to east (the marine region) around 12:00 CST, and the wind speed increased from 2 to 6 m s^{-1} . Correspondingly, the $\text{P}(\text{O}_x)$ decreased sharply from 19 to 5 ppbv h^{-1} , and the ambient O_x concentration at the site continued to increase and finally exceeded 100 ppbv at 15:00 CST. On the same day, the observed O_x concentration at night reached 80 ppbv. This suggested that the photochemically produced O_3 in the YRDR during the daytime was preserved over the marine area and was transported directly to the observation site with an easterly sea breeze at night.

On the morning of 22 June 2010 (as shown in Fig. 5b and e), the site experienced prevailing southwesterly winds, and the accumulated photochemical production of O_x (06:00–13:00 CST) was only 14 ppbv, accounting for one-fourth of the observed daytime O_x concentration buildup (60 ppbv), reflecting the importance of the direct transport of O_x .

5.2 Dependence of $\text{P}(\text{O}_x)$ sensitivity on the source region

The sensitivity of $\text{P}(\text{O}_x)$ to its precursor concentrations was investigated based on model simulations by artificially multiplying the NO_x concentration by factors of 0.5 and 2, while the NMHC concentration was kept unchanged, or by multiplying the NMHC concentration by a factor of 0.5, while the NO_x concentration remained unchanged. The sensitivity of the $\text{P}(\text{O}_x)$ on several O_3 pollution cases and their corresponding footprint regions was determined using a back trajectory model (Fig. 6). As shown in Fig. 4, the emission characteristics of O_3 precursors observed at the site differed for pollutants arising from different directions, resulting in distinct O_x production sensitivity. For the pollution that originated from the western inland area (Fig. 6a, b), $\text{P}(\text{O}_x)$ was very sensitive to variations in VOCs, and a decrease in NO_x led to an obvious increase in $\text{P}(\text{O}_x)$, even in the afternoon when NO_x had been significantly consumed, which suggested that $\text{P}(\text{O}_x)$ occurred in a typically VOC-limited regime. However, when the air masses originated from the north/coastal region

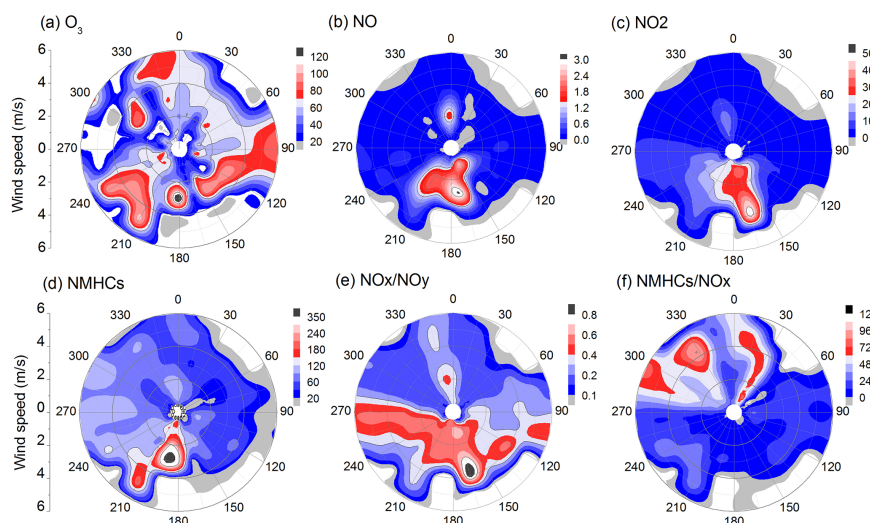


Figure 4. Dependence of the mixing ratios of (a) O_3 , (b) NO, (c) NO_2 , (d) NMHCs, (e) NO_x / NO_y , and (f) NMHCs/ NO_x on wind direction and speed.

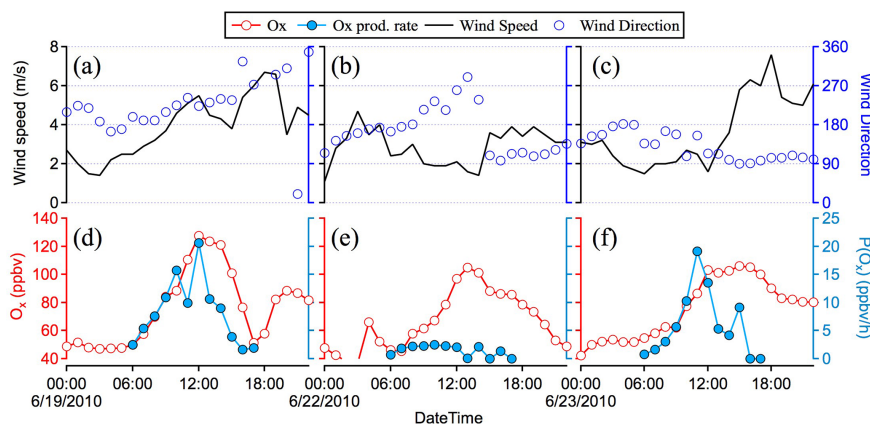


Figure 5. Diurnal variations in O_x concentration, $P(O_x)$, and wind speed and direction for three typical O_3 pollution cases on 19, 22, and 23 June during the field observation period.

(Fig. 6d), $P(O_x)$ was primarily controlled by ambient NO_x concentrations (Fig. 6c), as indicated by the extremely low NO_x concentration (average: 0.93 ppbv) and relatively high NMHC concentration (42.5 ppbv) during the daytime.

Most notably, we observed an obvious alteration in $P(O_x)$ sensitivity for the air mass transported from the south region (Fig. 6e and f). $P(O_x)$ on the morning of 19 June 2010, which was much more sensitive to the NMHC concentration than to NO_x , and an increase in NO_x concentration resulted in a decrease in $P(O_x)$ (VOC-limited regime). In the afternoon, the NO_x mixing ratio decreased significantly from 21.7 ppbv in the morning to 2.9 ppbv in the afternoon due to photochemical processes in the atmosphere, and the $P(O_x)$ became NO_x -limited, and a doubling of the NO_x concentration led to a clear increase in $P(O_x)$. Footprint analysis (Fig. 6f) indicated that the air masses were mostly stagnant over polluted regions in the YRDR, implying that anthropogenic pollution

emission from urban areas was a determinant in the variation in $P(O_x)$.

5.3 Isopleth diagram of $P(O_x)$

To better evaluate the $P(O_x)$ sensitivity to NMHCs and NO_x concentrations at the site, a series of model runs were performed that artificially decreased and increased the NO_x and NMHC concentration to cover wide areas and simulate real atmospheric conditions, as described in Sect. 5.2. The mixing ratios of O_3 , NO_x , and NMHCs, J values, and meteorological data observed at 10:00 CST on 19 June were used as constraints. The dependence of the $P(O_x)$ on NMHCs and NO_x is shown in Fig. 7. The circles in the plot represent the calculated $P(O_x)$ and the gray dashed line indicates variations in NO_x during the day. The model predicted that the ridge of the $P(O_x)$ was associ-

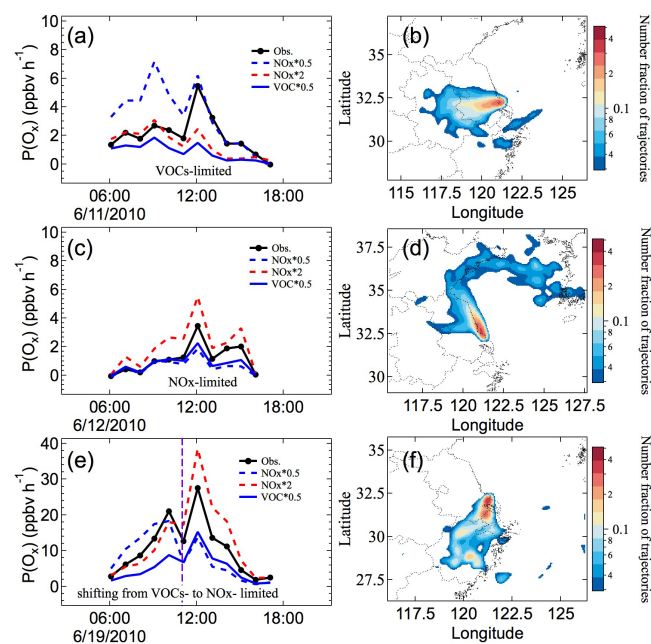


Figure 6. O_3 production sensitivity of the air masses with different footprint regions. The left panel shows the variation in the production rate of O_3 by artificial alteration of NO_x and VOCs; the right panel shows the number of trajectories that passed through the mixing layer for each case.

ated with an $NMHCs/NO_x$ ratio of 10–20 ppbC ppbv⁻¹, similar to the prediction of urban photochemistry in central Tokyo (Kanaya et al., 2008). In the morning, relatively low $NMHCs/NO_x$ ratios (~ 5 ppbC ppbv⁻¹) were found owing to a substantial amount of NO_x , and $P(O_3)$ approached the predicted “ridge” region due to the preferential presence of hydroperoxyl (HO_2) and peroxy radicals based on model calculations. In the afternoon, the $NMHC/NO_x$ ratio increased evidently up to 30–50 ppbC ppbv⁻¹ due to rapid NO_x photochemical loss. This tendency was generally consistent with the observation in the Shanghai urban area (Ran et al., 2009). Footprint analysis illustrated that the high concentration of $NMHCs$ in the air mass was associated with urban emissions in the YRDR. O_3 production on the morning of 23 June occurred in a typical VOC-limited regime ($NMHCs/NO_x$ ratio: ~ 1 ppbC ppbv⁻¹), and it gradually shifted to a NO_x -limited regime in the afternoon ($NMHC/NO_x$ ratio: 21 ppbC ppbv⁻¹ at 15:00 CST) due to a change in the wind direction.

5.4 Contributions of different sources to in situ $P(O_3)$

Source appointment of $NMHCs$ observed during the field campaign was attempted based on the PMF calculation, as described in Sect. 3.2. The data matrix for PMF was 206 rows (samples) \times 23 columns (species). The uncertainty in $NMHC$ concentrations was determined as the sum of 15 % of the concentration and half of the detection limit (the same

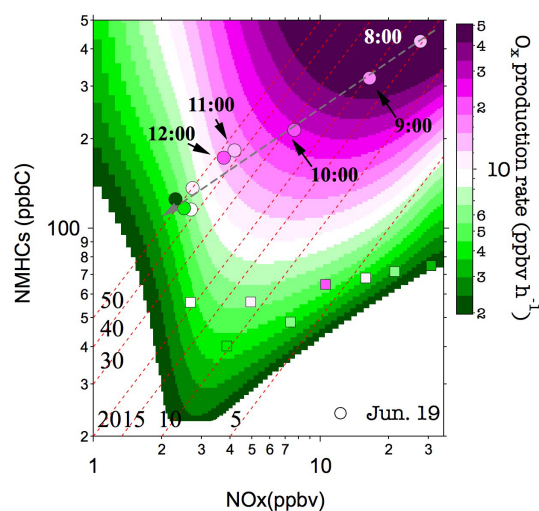


Figure 7. O_3 production isopleth plot derived from RACM sensitivity simulations at the observation site. The gray dashed line indicates the diurnal variation of the ambient NO_x concentration on 19 June 2010. The red dotted lines represent the ratio of $NMHC/NO_x$.

as the descriptions in the PMF user’s guide). Three potential factors were determined in this study. The contributions of the specified factor to each species are shown in the Supplement. Factor 1 showed an obvious diurnal variation and consisted of a large fraction of high-reactive species (e.g., C_8 – C_9 aromatics, 1-butene) and NO_2 . Factor 2 did not have diurnal variability and had an abundance of low-weight alkanes and fewer fractions of high-reactive species and NO_2 . As reported previously (Yuan et al., 2012), $NMHC$ photochemistry could lead to different time series for more and less reactive species, and PMF can detect these differences and attribute more or fewer reactive species to different factors, even though they originate from the same source. Therefore, we cannot identify the emission sources for these two factors. Instead, we attributed factors 1 and 2 to less-processed and more-processed air masses. Factor 3 was considered an OBB-related source due to the pronounced contribution of furan and acetonitrile with mass fractions of 64 and 50 %, respectively. This factor also accounted for 72 % of total isoprene, 51 % of $MVK + MACR$ (oxidation production of isoprene), and 52 % of acetic acid. As shown in previous studies (Kudo et al., 2014), factor 3 would retain the source characteristics, as the OBB occurred near the observation site.

The sensitivity of each source on $P(O_3)$ at the site was quantified as follows. The $NMHC$ and NO_x concentrations of one selected factor were artificially increased by 10 %, while the concentration of $NMHCs$ and NO_x for other factors remained unchanged. In such a situation, the total variation in $NMHC$ and NO_x concentrations was normally within 5 %, guaranteeing that the RACM calculation could be well constrained. The variation in $P(O_3)$ due to changes in the $NMHC$

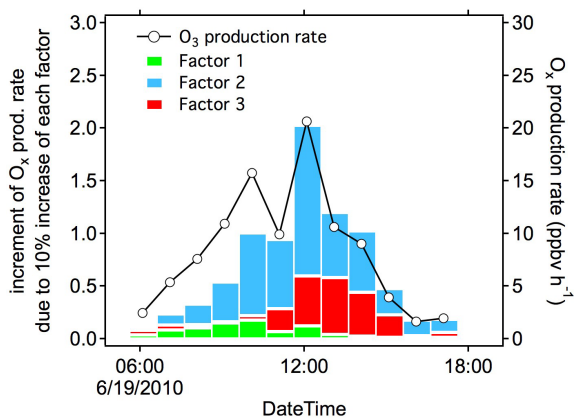


Figure 8. Diurnal variation in the sensitivity of each source to in situ O_x photochemical production and $P(O_x)$ on 19 June 2010.

and NO_x concentrations of selected factor was deemed the relative contribution of the factor to O_x formation. Here, we showed the relative importance of each factor on the in situ photochemical formation of O_x for a typical heavy O_3 pollution case on 19 June 2010 (hourly averaged O_3 concentration: 124 ± 5 ppbv and one minute value: 168 ppbv at 12:00 CST). As shown in Fig. 8, the contribution of different sources to O_x production showed distinct variation patterns. Factor 2 was responsible for 60 % (43 ppbv) of the in situ photochemical production of O_x in the morning, followed by that of factor 1 (23 %, 17 ppbv), and the OBB-related factor only accounted for 17 % of the total O_x production. In the afternoon, the relative importance of OBB-related factors increased and was responsible for 34 % (12 ppbv) of the photochemical O_x production.

5.5 Biogenic isoprene

In the present study, mean mass concentrations of isoprene and MVK+MACR (photo-oxidation products of isoprene) at the site were 0.2 ± 0.1 ppbv and 0.8 ± 0.6 ppb, respectively, with a mean MVK+MACR to isoprene ratio ($[MVK+MACR]/\text{isoprene}$) of 5.2. Biogenic sources (normally predominant at noon) were not mathematically resolved by the PMF calculation. Most of the isoprene was attributed to OBB sources and the rest was assigned to sources related to transport factors. First, the $[MVK+MACR]/\text{isoprene}$ ratio was normally less than 0.4 in the biogenic sources-dominant environment (Montzka et al., 1993). Yuan et al. (2012) reported that the mass ratio of $[MVK+MACR]/\text{isoprene}$ was 0.3 for biogenic sources based on PMF analysis. In the present study, the $[MVK+MACR]/\text{isoprene}$ ratio ranged from 3 to 25, suggesting that the impact of biogenic sources was not significant. Kudo et al. (2014) reported that observed normalized excess mixing ratios (NEMRs) of OVOCs increased with air mass age, suggesting that the isoprene may undergo

further oxidation after being emitted. The upper limit of the $[MVK+MACR]/\text{isoprene}$ ratio was ~ 30 in this study. Third, the observation site was located adjacent to a large wheat field, and wheat plants emit small amounts of isoprene (Kesselmeier and Staudt, 1999); the diurnal variation in isoprene at the site did not show a pronounced enhancement at noontime (10:00–15:00 CST), and the 6 h averaged isoprene concentration was 0.19 ± 0.16 ppbv. Based on these observations, we deemed that biogenic sources had limited impacts on in situ O_x production and were therefore neglected in the above discussion.

5.6 Impact of aerosols on O_x production

The presence of particles reportedly can result in a significant heterogeneous losses of HO_2 (Taketani et al., 2008), which plays a key role in peroxy radical equilibrium and O_3 formation in the troposphere. The study at the mountain site in central East China indicated that ambient HO_2 concentrations and corresponding $P(O_x)$ decreased due to the heterogeneous loss of HO_2 (Kanaya et al., 2009). In the present study, the effect of a heterogeneous loss of HO_2 on the $P(O_x)$ was investigated. The loss rate of HO_2 was calculated using the Fuchs–Sutugin equation (Kanaya et al., 2009). The gas-phase diffusion coefficient of HO_2 was assumed to be $0.247 \text{ cm}^2 \text{ s}^{-1}$. The dependence on the uptake coefficient of HO_2 on relative humidity (ranging from 0.2 to 0.35) was considered based on laboratory studies (Taketani et al., 2008). The number size distribution of particles (size bins: 0.3–0.5, 0.5–0.7, 0.7–1.0, 1.0–2.0, 2.0–5.0 μm) during the campaign was measured using a portable particle counter (model KR-12A; RION Inc.). As a result, the estimated loss rate of HO_2 ranged from $7 \times 10^{-3} \text{ s}^{-1}$ to 0.05 s^{-1} . The incorporation effect of HO_2 loss into the RACM model calculation resulted in a reduction of $P(O_x)$ by 13 % on average. Huang et al. (2011) reported that primary anthropogenic emissions of $PM_{2.5}$ and PM_{10} in the YRDR were 1511 and 3116 Gg yr^{-1} in 2007, respectively, accounting for 11 and 17 % of the total emissions in China. This suggested that O_3 photochemical production might have been depressed due to the presence of aerosol particles in the atmosphere. Our hypothesis was supported by a previous report (Gerasopoulos et al., 2013), which showed that JO^1D decreased by 40 % at a high solar zenith angle during high aerosol loading periods ($AOD = 0.5\text{--}0.7$). Presumably, ambient O_3 concentrations would increase provided that particle emissions are significantly reduced, while NO_x and NMHCs emissions remain unchanged. Moreover, variability in meteorological conditions affects O_3 production. For example, an increase in relative humidity could lead to a more rapid heterogeneous loss of HO_2 on the wet surface of particles (Taketani et al., 2008). To summarize, accounting for the impact of aerosols is extremely important in reviewing and predicting O_3 pollution in East Asia under the scenario of global warming.

6 Conclusions

To investigate the impact of OBB on O₃ pollution, a field campaign on O₃ and its precursors was performed in a rural area of the YRDR during the harvest season in 2010. A photochemical box model (RACM version 2) was used to investigate the O_x production rate, controlling regime, and its possible contributors. Our study demonstrated that O_x pollution exacerbated when the site was subjected to both the OBB plumes and urban pollution in the YRDR. During a high-O₃ pollution period (19 June 2010), the diurnal variation in O_x production rates had a maximum value of 21 ppbv h⁻¹, with an accumulated O_x production rate of 100 ppbv on a daily basis. *in situ* photochemical production could almost fully explain the buildup of O_x in the morning at the site. Direct transport was also important for the ambient O_x level at the site, especially in the afternoon. O_x production sensitivity differed for the air masses arising from different directions due to distinct emission characteristics. When air masses originated from the urban/industrial areas to the south of the observation site, O_x production was NMHC-limited in the morning but became NO_x-limited in the afternoon due to a significant depletion in NO_x. According to PMF analysis, the contributions of three identified factors (less-processed, more-processed, and OBB-related sources) to *in situ* O_x production were evaluated. We found that less-processed and more-processed air masses were responsible for 83 % of the photochemical production of O_x in the morning, and OBB-related factors accounted for 34 % of O_x production in the afternoon. Biogenic isoprene emissions were found to be less important for O_x production at the site during our study period. Our results implied that reductions in NMHCs, NO_x, and OBB control measures in the YRDR are important for reducing the risk of high-O₃ pollution events.

The Supplement related to this article is available online at doi:10.5194/acp-15-6101-2015-supplement.

Acknowledgements. The authors thank the staff of the Rudong Municipal Environment Protection Bureau who provided us with assistance and facilitated the preparation and implementation of the field campaign. This work was supported by the Environment Research and Technology Development Fund (S-7, C-081, B-051) from the Ministry of the Environment, Japan.

Edited by: M. Shao

References

- Cape, J.: Surface ozone concentrations and ecosystem health: Past trends and a guide to future projections, *Sci. Total Environ.*, 400, 257–269, doi:10.1016/j.scitotenv.2008.2008.
- Goliff, W. S., Stockwell, W. R., and Lawson, C. V.: The regional atmospheric chemistry mechanism, version 2, *Atmos. Environ.*, 68, 174–185, doi:10.1016/j.atmosenv.2012.11.038, 2013.
- Hao, N., Valks, P., Loyola, D., Cheng, Y. F., and Zimmer, W.: Space-based measurements of air quality during the World Expo 2010 in Shanghai, *Environ. Res. Lett.*, 6, 044004, doi:10.1088/1748-9326/6/4/044004, 2011.
- Hornbrook, R. S., Blake, D. R., Diskin, G. S., Fried, A., Fuelberg, H. E., Meinardi, S., Mikoviny, T., Richter, D., Sachse, G. W., Vay, S. A., Walega, J., Weibring, P., Weinheimer, A. J., Wiedinmyer, C., Wisthaler, A., Hills, A., Riemer, D. D., and Apel, E. C.: Observations of nonmethane organic compounds during ARC-TAS – Part 1: Biomass burning emissions and plume enhancements, *Atmos. Chem. Phys.*, 11, 11103–11130, doi:10.5194/acp-11-11103-2011, 2011.
- Kanaya, Y., Fukuda, M., Akimoto, H., Takegawa, N., Komazaki, Y., Yokouchi, Y., Koike, M., and Kondo, Y.: Urban photochemistry in central Tokyo: 2. Rates and regimes of oxidant (O₃+ NO₂) production, *J. Geophys. Res.-Atmos.*, 113, D06301, doi:10.1029/2007JD008671, 2008.
- Kanaya, Y., Pochanart, P., Liu, Y., Li, J., Tanimoto, H., Kato, S., Suthawaree, J., Inomata, S., Taketani, F., Okuzawa, K., Kawamura, K., Akimoto, H., and Wang, Z. F.: Rates and regimes of photochemical ozone production over Central East China in June 2006: a box model analysis using comprehensive measurements of ozone precursors, *Atmos. Chem. Phys.*, 9, 7711–7723, doi:10.5194/acp-9-7711-2009, 2009.
- Kesselmeier, J. and Staudt, M.: Biogenic volatile organic compounds (VOC): an overview on emission, physiology and ecology, *J. Atmos. Chem.*, 33, 23–88, doi:10.1016/j.jqsrt.2014.08.003, 1999.
- Kudo, S., Tanimoto, H., Inomata, S., Saito, S., Pan, X., Kanaya, Y., Taketani, F., Wang, Z., Chen, H., Dong, H., Zhang, M., and Yamaji, K.: Emissions of nonmethane volatile organic compounds from open crop residue burning in the Yangtze River Delta region, China, *J. Geophys. Res.-Atmos.*, 119, JD021044, doi:10.1002/2013JD021044, 2014.
- Kurokawa, J., Ohara, T., Morikawa, T., Hanayama, S., Janssens-Maenhout, G., Fukui, T., Kawashima, K., and Akimoto, H.: Emissions of air pollutants and greenhouse gases over Asian regions during 2000–2008: Regional Emission inventory in ASia (REAS) version 2, *Atmos. Chem. Phys.*, 13, 11019–11058, doi:10.5194/acp-13-11019-2013, 2013.
- Montzka, S. A., Trainer, M., Goldan, P. D., Kuster, W. C., and Fehsenfeld, F. C.: Isoprene and Its Oxidation-Products, Methyl Vinyl Ketone and Methacrolein, in the Rural Troposphere, *J. Geophys. Res.-Atmos.*, 98, 1101–1111, doi:10.1029/92JD02382, 1993.
- Pan, X., Kanaya, Y., Wang, Z., Taketani, F., Tanimoto, H., Irie, H., Takashima, H., and Inomata, S.: Emission ratio of carbonaceous aerosols observed near crop residual burning sources in a rural area of the Yangtze River Delta Region, China, *J. Geophys. Res.-Atmos.*, 117, D22304, doi:10.1029/2012JD018357, 2012.
- Pan, X. L., Kanaya, Y., Wang, Z. F., Liu, Y., Pochanart, P., Akimoto, H., Sun, Y. L., Dong, H. B., Li, J., Irie, H., and Takigawa,

- M.: Correlation of black carbon aerosol and carbon monoxide in the high-altitude environment of Mt. Huang in Eastern China, *Atmos. Chem. Phys.*, 11, 9735–9747, doi:10.5194/acp-11-9735-2011, 2011.
- Pan, X. L., Kanaya, Y., Wang, Z. F., Komazaki, Y., Taketani, F., Akimoto, H., and Pochanart, P.: Variations of carbonaceous aerosols from open crop residue burning with transport and its implication to estimate their lifetimes, *Atmos. Environ.*, 74, 301–310, 2013.
- Ran, L., Zhao, C., Geng, F., Tie, X., Tang, X., Peng, L., Zhou, G., Yu, Q., Xu, J., and Guenther, A.: Ozone photochemical production in urban Shanghai, China: Analysis based on ground level observations, *J. Geophys. Res.-Atmos.*, 114, D15301, doi:10.1029/2008JD010752, 2009.
- Sitch, S., Cox, P., Collins, W., and Huntingford, C.: Indirect radiative forcing of climate change through ozone effects on the land-carbon sink, *Nature*, 448, 791–794, 2007.
- Stockwell, W. R., Kirchner, F., Kuhn, M., and Seefeld, S.: A new mechanism for regional atmospheric chemistry modeling, *J. Geophys. Res.*, 102, 25847–25879, 1997.
- Takegawa, N., Kondo, Y., Ko, M., Koike, M., Kita, K., Blake, D., Hu, W., Scott, C., Kawakami, S., and Miyazaki, Y.: Photochemical production of O₃ in biomass burning plumes in the boundary layer over northern Australia, *Geophys. Res. Lett.*, 30, 1500, doi:10.1029/2003GL017017, 2003.
- Taketani, F., Kanaya, Y., and Akimoto, H.: Kinetics of heterogeneous reactions of HO₂ radical at ambient concentration levels with (NH₄)₂SO₄ and NaCl aerosol particles, *J. Phys. Chem. A*, 112, 2370–2377, 2008.
- Wang, T., Ding, A., Gao, J., and Wu, W. S.: Strong ozone production in urban plumes from Beijing, China, *Geophys. Res. Lett.*, 33, L21806, doi:10.1029/2006GL027689, 2006.
- Wang, T., Wei, X. L., Ding, A. J., Poon, C. N., Lam, K. S., Li, Y. S., Chan, L. Y., and Anson, M.: Increasing surface ozone concentrations in the background atmosphere of Southern China, 1994–2007, *Atmos. Chem. Phys.*, 9, 6217–6227, doi:10.5194/acp-9-6217-2009, 2009.
- Xu, X., Lin, W., Wang, T., Yan, P., Tang, J., Meng, Z., and Wang, Y.: Long-term trend of surface ozone at a regional background station in eastern China 1991–2006: enhanced variability, *Atmos. Chem. Phys.*, 8, 2595–2607, doi:10.5194/acp-8-2595-2008, 2008.
- Yamaji, K., Li, J., Uno, I., Kanaya, Y., Irie, H., Takigawa, M., Komazaki, Y., Pochanart, P., Liu, Y., Tanimoto, H., Ohara, T., Yan, X., Wang, Z., and Akimoto, H.: Impact of open crop residual burning on air quality over Central Eastern China during the Mount Tai Experiment 2006 (MTX2006), *Atmos. Chem. Phys.*, 10, 7353–7368, doi:10.5194/acp-10-7353-2010, 2010.
- Yuan, B., Shao, M., Gouw, J., Parrish, D. D., Lu, S., Wang, M., Zeng, L., Zhang, Q., Song, Y., and Zhang, J.: Volatile organic compounds (VOCs) in urban air: How chemistry affects the interpretation of positive matrix factorization (PMF) analysis, *J. Geophys. Res.-Atmos.*, 117, D24302, doi:10.1029/2012JD018236, 2012.
- Zhang, Q., Streets, D. G., Carmichael, G. R., He, K. B., Huo, H., Kannari, A., Klimont, Z., Park, I. S., Reddy, S., Fu, J. S., Chen, D., Duan, L., Lei, Y., Wang, L. T., and Yao, Z. L.: Asian emissions in 2006 for the NASA INTEX-B mission, *Atmos. Chem. Phys.*, 9, 5131–5153, doi:10.5194/acp-9-5131-2009, 2009.
- Ziemke, J., Chandra, S., Duncan, B., Schoeberl, M., Torres, O., Damon, M., and Bhartia, P.: Recent biomass burning in the tropics and related changes in tropospheric ozone, *Geophys. Res. Lett.*, 36, L15819, doi:10.1029/2009GL039303, 2009.